An Enhanced Model for Evaluating Failure Propagation in Launch Vehicle Engine Sections

Susie Go[a], Scott Lawrence[a], and Amir Levine[b]
[a] NASA Ames Research Center, Moffett Field, USA, Susie.go@nasa.gov, scott.l.lawrence@nasa.gov
[b] Amir organization, City, Country, Email address

Abstract: An important component in the assessment of launch vehicle safety is the estimation of the likelihood of large-scale explosions given the existence of failures that manifest as a localized energy release. A failure propagation model is presented for simulating cascading failures of energetic components in proximity where the primary modes of energy transfer are fragments/shrapnel and blast overpressure. The model is an extension of the model developed by Mathias and Motiwala (2015) [1] with enhancements to include the effects of fragment ricochet, fragment drag, fragment ballistic limit equation thresholds, and blast impulse thresholds. A series of sensitivity studies were conducted for a generic launch vehicle engine section and results are presented that illustrate the effects of the model modifications.

1. INTRODUCTION

Traditional risk and safety assessments often use fault tree and event tree methods as the primary analysis tool. These methods were originally developed for use in accident investigations and functioned well for analyzing existing complex engineering systems to identify possible root causes of an accident. However, the static nature of fault trees and event trees make them extremely difficult to use as an analysis tool for studying time-dependent failure scenarios, when the prevailing conditions are rapidly changing or the topology of the original system is evolving, as in space launch systems. These methods tend to be based on the functional relationships among the system components, while failure propagation in highly energetic systems is often strongly driven by proximity-based physics.

The goal of this effort is a capability for estimating failure evolution from component engineering information, specifically geometric data, and information describing the relationships between components (a small set of local failure breakup assumptions and critical component damage criteria). This minimized the reliance on detailed design data, something that is often unavailable during the early conceptual design phases. The failure propagation methodology and associated C++ code were first described in Mathias & Motiwala, 2015 [1] and has been updated with newer blast physics and debris penetration models. The current model includes the effects of fragment ricochet, i.e., fragments being redirected after impact with non-punctured components to potentially cause the failure of other components. This increased the fidelity of the debris model relative to the initial approach, which assumed components that were struck, but not damaged, would absorb those fragments.

A challenging problem in the safety assessment of a crewed launch vehicle system is the estimation of the consequences from uncontained engine failure within a multi-engine engine bay. In assessing the ability of a crew to successfully escape such a failure, a critical factor is the likelihood that the initial failure will propagate to other engines or rupture the adjacent propellant tank. The current risk model uses readily available component design information to track component states after an initial engine failure and couples these states to component responses based on blast wave and debris cloud propagation models. The dynamic time evolution of the component failure status is tracked, producing self-generated event trees. Stochastic application of this process, driven by uncertain inputs, provides useful probabilistic insight into design elements contributing to crew risk. In this paper, the model will be applied to a generic launch vehicle engine section with the objective of understanding the impact of the recent model enhancements on figures of merit related to vehicle safety.

2. MODELING APPROACH

The propagation model consists of the elements shown in Figure 1:

1. Vehicle configuration: geometries and locations of its major components. This is currently implemented using CAD-based triangulated component surfaces.
2. Component design specification: physical and operational parameters that describe the components. Examples include wall thickness, wall material, operating pressure, temperature, volume, turbine spin rates, etc.
3. Supplemental component failure assumptions: parameters characterizing the blast and debris environments generated when the component fails, as well as the capability to resist imposed blast and debris environments. These parameters are typically provided as uncertain distributions from which the Monte Carlo process selects specific input sets.
4. Physical environment propagation models: models to express the propagation, spatially and temporally, of the failure environments from initiation to interaction with target components, e.g., decay of blast overpressure with distance. The models account for environmental conditions, e.g., ambient pressure, at the time of the failure, and component design and failure information.
5. Monte Carlo Propagation model: logic to stochastically sample uncertain input parameters related to the initiation of failure environments, manage the evolution of the failure propagation process by tracking the component states (failures) over time, and accumulate data from the sample runs.
6. Outputs: detailed component failure sequences and global timelines for each Monte Carlo realization, as well as probabilistic data from the averaged results over the entire experiment.

Figure 1. Failure propagation model inputs and outputs: vehicle definition (green), physical modeling parameters (blue), failure environment parameters (yellow), propagation model (center), and outputs (grey).

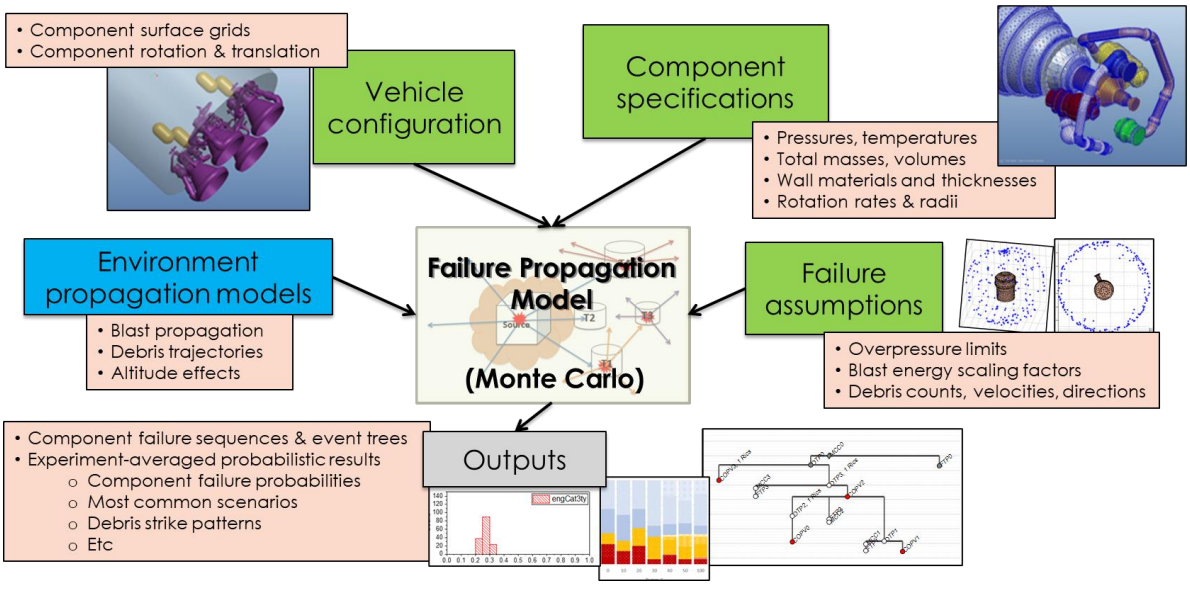

An example failure scenario begins with an "uncontained" failure in a user-specified, high-energy component. This will release a blast wave and/or debris cloud that propagates to the other components in the engine bay. If the overpressure and/or debris environments exceed failure thresholds, then the impacted components also fail. This will create a naturally propagating failure path based on the self-evolving scenario. The failure propagation code maintains a list of failed components and their times

of failure and continually sorts the list to ensure chronological consistency. The dependence on design information and physics-based modeling minimizes the use of reliability data. No *a priori* event sequences or logic gates are needed, as the code evolves the failure paths based only on the physics of the problem, the failure criteria, and the integrated system state.

Under the Monte Carlo logic, the above process is stochastically applied with input sets selected randomly from the user-specified distributions. As currently written, the model only expects uncertainties in the characterization of the component failure environments, e.g., number of fragments generated, overpressure failure threshold, etc.

Results are then expressed as probabilities of failure of each of the system components. Additional outputs are computed to further the understanding of potential outcomes from the initial failure. At the most detailed level, each Monte Carlo sample is available in the form of an event tree, including such information as failure source, failure target, failure time (from initial component failure), and failure mode (overpressure, debris).

3. PHYSICAL MODELING

The following subsections describe the two primary physical models, the debris model and the blast overpressure model. The descriptions detail the recent enhancements added to each model.

3.1 Debris Model

In the original propagation model [1], a component failure resulting in a debris cloud has the debris particles initially positioned at the centroid of the failed component. The debris cloud piece count, initial particle speed and mass were defined by the user as probabilistic distributions. The shape of the debris cloud depended on the component type. For components with high rotational kinetic energy, such as turbomachinery, the debris cloud was expected to take a diffused disk-like "Blade" form distribution, compared to uniform spherical distributions for the other energetic components (Figure 2).

Figure 2. Comparison of debris velocity direction distributions.

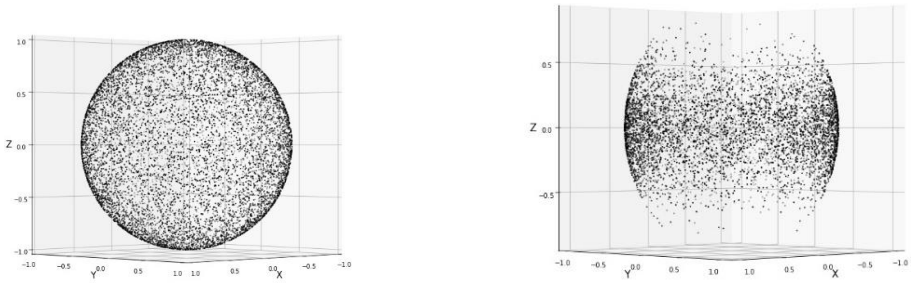

a) Spherical distribution b) "Blade" distribution

Debris piece velocities were calculated using a simple model based on case burst fragmentation (for case burst failures) or using the turbine radius and rotation rate (for turbo-machinery failures), with the debris travelling along linear trajectories at a constant velocity. A failure of an impacted component was triggered when the kinetic energy of the debris piece exceeded a user-defined threshold for the impacted component.

Three modifications were made to the original debris model. The effects of drag on the debris piece velocities were included. A material-based failure criteria (ballistic limit equation) was implemented. Finally, a model to represent fragment ricochet after an impact was incorporated. Drag effects were found to have minimal effect in the present application and the drag decay modeling will not be described here.

3.1.1 Failure Criteria

The current debris model contains two different options to define the failure limit: a simple failure definition based on the kinetic energy of a particle and an empirically-based penetration formula. Either of these approaches can be expressed in terms of a limiting impact velocity.

The original code only used the kinetic energy limit approach, in which the limiting kinetic energy, KE_{lim}, is specified and the failure velocity V_{lim} is evaluated as $V_{lim} = \sqrt{2 \cdot KE_{lim} / m}$, where *m* is the mass of debris fragment.

The current model includes an empirically-based penetration criteria based on the penetration equations developed by the Office of Aviation Research and Development [2,3]. Based on test data, the ballistic response was characterized via the shear strength constant (formerly dynamic shear modulus), within the penetration equations.

The penetration equation, known as the Federal Aviation Administration (FAA) ballistic limit equation (BLE), is given by: $V_{50} = \sqrt{2LC_s t^2 / (m \cos^2 \theta)}$. Here, V_{50} is the limit velocity, L is the perimeter of the fragment projected area, C_s is the shear strength constant of the target material, t is target wall thickness, m is the fragment mass, and θ is the obliquity of the impact (90 deg is perpendicular). The fragment perimeter is not typically a direct output of fragmentation assumptions and must be estimated in terms of other parameters, such as total component area and fragment count. The impact angle is calculated as the angle between the ray from the centroid of the source component and the plane defined by a target component surface mesh element.

3.1.2 Ricochet

In the previous version of the model, if the debris failure threshold was not exceeded, debris fragments were absorbed by the impacted component, thus ending their individual failure event chains. A ricochet model has been implemented in the current version which deflects these fragments based on their velocity, impact angle and coefficient of restitution (Figure 3). The following equation was used to determine the redirected velocity of the debris fragment:

$$\boldsymbol{V} = \boldsymbol{V_0} - (1 + C_R) * (\boldsymbol{V_0} \circ \boldsymbol{P})\widehat{\boldsymbol{P}}$$

where

$\boldsymbol{V}$ = Fragment's redirected velocity (m/s)
$\boldsymbol{V_0}$ = Fragment's original velocity (m/s)
C_R = Coefficient of Restitution
$\boldsymbol{P}$ = Vector normal to the plane of the triangulated surface (m)

For computational efficiency, and to avoid the possibility of "ringing" between flat component faces, a limit on the number of ricochets a given fragment may undergo was imposed.

Figure 3. Ricochet example assuming $\boldsymbol{C_R = 0.8}$.

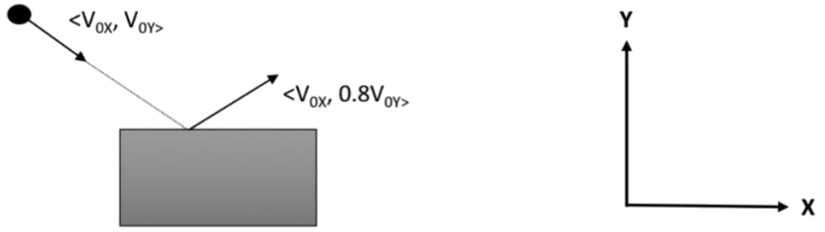

Ricochet enabled more realistic debris propagation. The energy from non-puncturing fragments remained within the system, potentially causing failure to other components. The effects of including

ricochet and of varying ricochet-related parameters on the results will be discussed in a subsequent section of this article.

3.2 Overpressure Model

A failed component could also generate a blast wave that propagated outward from its centroid. This overpressure environment was represented using a standard TNT blast model (Kingery-Bulmash) [4] in the current version of the model. This model was chosen for its relative simplicity and efficiency, even though the TNT blast model would typically be conservative in comparison with a true pressure-vessel burst, especially near the blast center.

The Kingery-Bulmash model used a curve fit for the decay of scaled overpressure, $(p_{peak} / p_\infty - 1)$, with distance from the blast center. The distance was scaled using the standard Sachs distance scale factor $\alpha = (E / p_\infty)^{1/3}$. In these relations, $p_\infty$is the ambient pressure, p_{peak} is the maximum pressure observed in the blast pressure signature, and E is the blast energy. As such, a single curve can be used to represent any number of blast events characterized by the estimated blast energy (E) and the ambient pressure (p_∞) at the altitude at which the failure occurred. The implication of the scaling by ambient pressure was that blast overpressure failures were reduced at higher altitudes as the ambient pressure decreased.

A shortcoming of the TNT blast model as applied to the present problem was the over-estimation of peak pressures in the very near-field of the blast. Two modifications were incorporated into the failure propagation blast model to address this short-coming. First, the pressures returned by the TNT model were limited by the pressure produced by the shock emanating from a shock tube with reservoir conditions set to the conditions of the failed component. Second, the integrated impulse was considered when assessing the failure status of target components. As a result, some nearby components exposed to high peak overpressures could survive because of the short duration of the blast wave exposure. The decay of integrated impulse was also available in the Kingery-Bulmash curve set, as was the time of arrival. The latter was included in the model to estimate the time between the source failure and target failure.

In this model, blasts were assumed to initiate at the source component centroid and expand spherically outward to the target component. There was no accounting for the shadowing effects of intermediate components. The components were assumed to be sufficiently distinct that the incident shock was able to refract around one component and re-join before encountering the next component.

4. TEST APPLICATION: GENERIC LAUNCH VEHICLE ENGINE SECTION

The following subsections describe the characteristics of the test application, the sensitivity case input parameters, and the results obtained from the simulations.

4.1. Configuration Description

The current model was used to analyze the launch vehicle engine bay described in (Mathias & Motiwala, 2015) [1]. This volume contained four identical liquid rocket engines, based on a highly simplified version of Aerojet Rocketdyne's J-2X engine, and four high-pressure helium Composite Overwrapped Pressure Vessels (COPVs) located between and above the engines. Each engine was clocked 90 degrees counterclockwise from its neighbor on the right (see **Error! Reference source not found.**4).

Each simplified engine consisted of seven engine components: a main combustion chamber (MCC), a fuel turbopump (FTP), an oxidizer turbopump (OTP), a nozzle, and 3 feed lines (fuel, oxidizer and hot gas). The MCC, FTP and OTP components and COPVs were assumed to be highly energetic, meaning failure of any of these components generated a blast overpressure wave and debris. The engine nozzles and pipes were not classified as high energy components, meaning failure of these components did not

propagate hazards to other components. Debris penetrations of non-energetic components were considered to be absorbed. Non-penetrating debris ricocheted if the maximum ricochet threshold was not reached.

Figure 4. Sample launch vehicle engine bay, includes 4 liquid rocket engines and 4 helium tanks. Each engine consists of 7 components: a main combustion chamber (MCC), fuel turbopump (FTP), oxidizer turbopump (OTP), nozzle, and three feed lines.

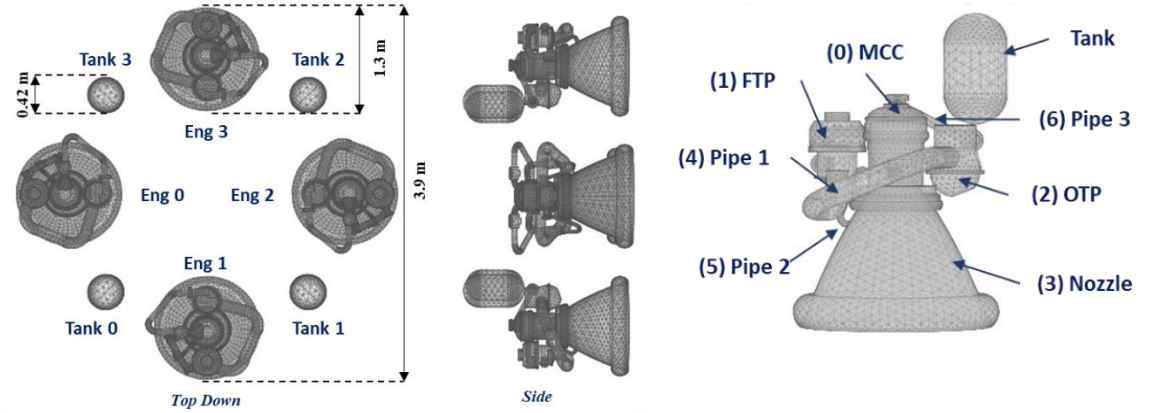

The triangulated surfaces shown in Figure 4 provided a description of the component geometries and the relative positions of the components. The analysis also required engineering properties of the components to characterize the behavior of the components within the failure environments. The design parameter inputs include:

- Component contents: Internal pressure, temperature, volume, and ratio of specific heats
- Component casing: Mass, wall thickness, wall material
- For turbomachinery components: Blade: mass (/blade), thickness, chord length, rotation radius, and spin rate

The list of failure propagation inputs include(parameters input as uncertain are indicated by [uncertain]:

- Failure mode: type of failure the component will experience: Case (pressure-vessel burst) versus Blade (turbopump blade release).
- Blast overpressure environment-related:
  - Fraction of contained energy that contributes to blast wave [uncertain]
  - Failure threshold (peak overpressure and impulse)
- Debris environment-related
  - Debris mass fraction: fraction of case/blade mass released as debris [uncertain]
  - Number of debris pieces produced [uncertain]
  - Debris velocity: scale factor [uncertain] applied to the velocity associated with the energy contained in the source system. For case failures, this is the confined gas energy and for blade failures, this is the kinetic energy of the attached blade.
  - Debris direction: directional debris release pattern

4.2. Description of Sensitivity Cases

The sensitivity of model results to various numerical parameters, physical modeling assumptions, and engineering property inputs were studied using the engine bay geometry described in the previous section. Sensitivity studies for the following parameters were performed:

1) Initiating component. Computations were performed starting with each energetic component of each engine as the initiating failure.
2) Number of Monte Carlo samples. Computations were performed for failure initiated by engine 0 main combustion chamber for Monte Carlo samples ranging from 1000 to 50,000.
3) Ricochet. Computations were performed varying the following two ricochet input parameters:
    a. Max number of ricochets
    b. Coefficient of restitution
4) Blast overpressure sensitivity. Computations were performed for various combinations of the altitude of failure, peak overpressure thresholds, and overpressure impulse thresholds.

4.3. Application Results

The results of the model sensitivity analysis are presented in the following sections.

4.3.1 Sensitivity to initiating component

The engine bay configuration had a high degree of symmetry with respect to both the engine components and the COPV placement. A sensitivity analysis was performed to verify that the simulations produce symmetric results with respect to the failure of energetic components of the four engines. Simulations each using 50000 Monte Carlo samples, were computed with failures of each of the first 12 components of the model. Results showed that the failure event trees generated by the Monte Carlo samples reflected the symmetry of the configuration. Therefore, a single engine (engine 0) was used as the failure initiator for subsequent studies.

4.3.2 Sensitivity to the number of Monte Carlo run samples

For this test case, six Monte Carlo experiments were performed with MCC0 as the failure initiator and sample sizes of 1000, 2000, 5000, 10000, 20000, and 50000. From each experiment, unique scenarios types (failed target/source pair lists) were identified and the number of Monte Carlo samples that contained each type were determined. The unique types were then ordered according to their likelihood and summed cumulatively, from most likely to least likely. The results of this process are plotted in Figure 5a for each of the six Monte Carlo experiments. The curves represent the cumulative density functions (CDF), showing that the effect of higher numbers of samples was to fill out the "tail" of the distribution.

Figure 5b plots the number of additional failed components, i.e., the number of nodes on the event tree, of each of the unique scenarios identified. Together, Figures 5a and 5b indicate that the most likely outcome of the initial failure was a single-node event tree, which occurred in ~40% of the samples. From Figure 5a, one also observes that approximately 70% of the outcomes are captured within the 10 most likely scenarios.

The failure propagation code produced data for each sample sufficient to provide a detailed description of the sequence of events. This information can be useful in understanding the sources of non-intuitive trends that arise in an investigation. For example, the event sequences can be used to identify intermediate components that contribute to the failure of a given component of interest.

Of particular interest are the failure probabilities of other energetic components after the initial failure. Figure 6 shows the sensitivity of those probabilities to the number of Monte Carlo samples. Also included are error bars evaluated using the standard central-limit-theorem formula for the 99% confident interval: $E = \pm 2.58\sqrt{\frac{P(1-P)}{nMC}}$. Here, P is the failure probability and nMC is the number of Monte Carlo samples in the run. As expected, higher sample counts produced results within the error bars of those using lower sample counts.

Figure 5. Interpreting the Monte Carlo set scenario composition and sensitivity to the number of samples.

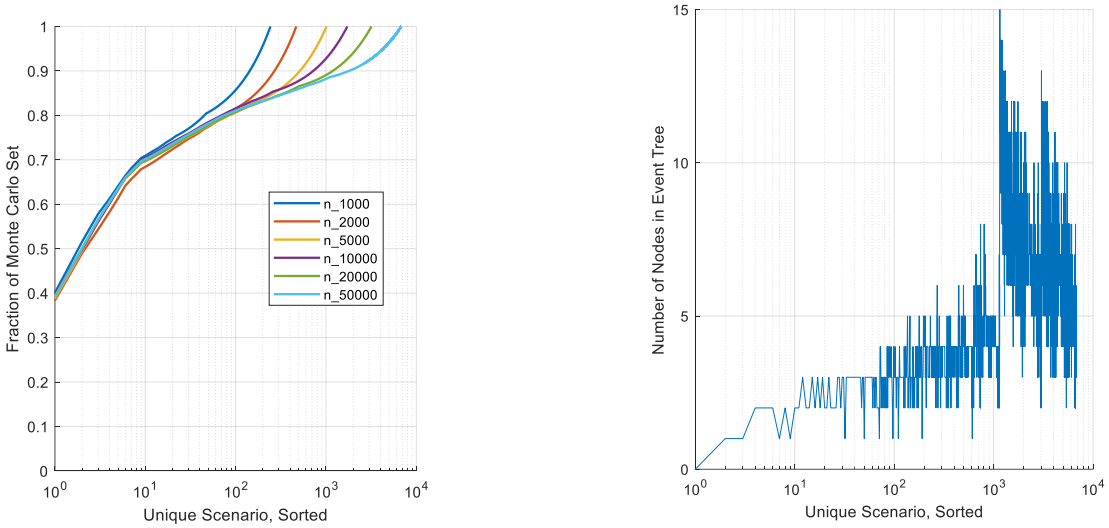

a. Cumulative distribution of scenario occurrence. b. Variation of scenario complexity.

Figure 6. Sensitivity of energetic component failure probabilities to the number of samples.

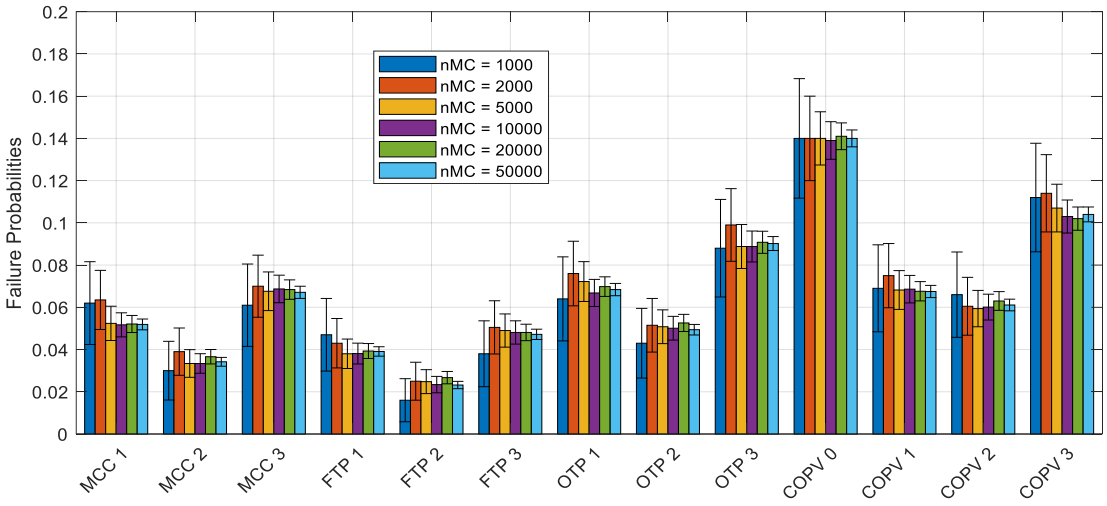

4.3.3 Sensitivity to ricochet model assumptions

Fragment ricochet was the most significant recent update to the current model. Parameters introduced with this model included: a) the number of ricochets allowed (maxRicochet), and, b) the global coefficient of restitution of the ricochet (C_r). In each Monte Carlo experiment, a constant value of C_r for all impacts was used. The impact of this assumption and the limit on the ricochet count are explored in the following sections.

Max Ricochet Count

In the model, a limit was placed on the number of times a particular fragment was allowed to ricochet. The default value was set at maxRicochet = 3. The sensitivity of the model to the value of maxRicochet was conducted.

Results were obtained for four values of maxRicochet using 50,000-sample Monte Carlo experiments and were assessed in terms of the failure probabilities of the energetic components, as shown in Figure

7. In the legend of Figure 7, n is used to represent maxRicochet. The results showed that for all components, a significant increase in failure probability was obtained when a single ricochet was allowed (n = 1). Additional ricochets produced diminishing increases in component failure probabilities. The increase in component failure probability between 1 and 3 ricochet cases were, with a few exceptions, within the 99% confidence error bars.

Another view of the results was provided by including an auxiliary component in the simulation and tracking the location of debris strikes on this "detection" component. For this configuration, a triangulated sphere was included. Figure 8 shows results of the ricochet sensitivity in terms of hit densities (hits per steradian, averaged over the full set of Monte Carlo samples) on this outer sphere. The sphere has been made partially transparent so that the other components inside the sphere can be seen.

Figures 8a-8c shows the sensitivity of the direction of the debris exiting the engine section to the ricochet assumptions. Figure 8a shows the results when no propagations were allowed (no ricochet and no additional component failures). This mode of operation was useful for computing view factors of various components with respect to the source component. In this case, there were distinct shadows on the detection sphere produced by the components surrounding the failure source. When propagation was enabled without ricochet (Figure 8b), the failure of the immediately adjacent turbopump produced debris dispersed around the "equator", filling in the shadow observed in Figure 8a. This dispersion was made non-uniform by the presence of additional blocking components and debris from additional component failures. Also observed was a generally higher level of hit density, relative to Figure 8a, associated with the additional debris being generated. Introducing ricochet produced still higher levels of hit densities as either because additional failures are generated by the ricochet fragments or because these fragments ultimately strike the sphere.

Figure 7. Sensitivity of energetic component failure probabilities to number of ricochets allowed, i.e., maxRicochet (n in legend).

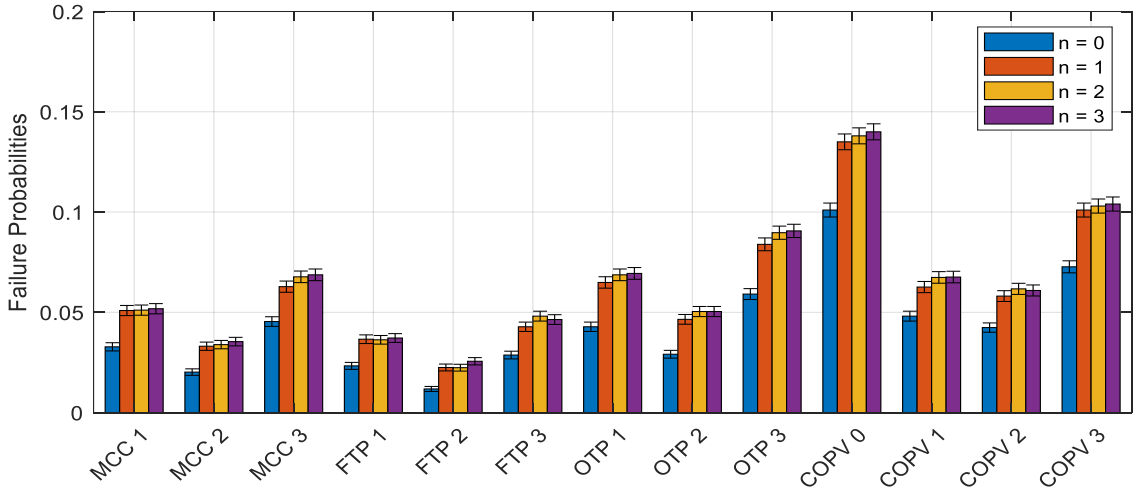

Coefficient of restitution

In this study, the coefficient of restitution (C_r) was varied from 0.2 to 1 (specular reflection), with maxRicochet set to 3. Results for the lowest value of C_r were virtually the same as the "no ricochet" case (n = 0) plotted in Figure 7. The $C_r = 0.8$ case was plotted in Figure 7 as the purple bars (n = 3). Intermediate values of C_r produced intermediate values for failure probability. Finally, the case of $C_r = 1$ (specular reflection) produced failure probabilities up to 5% higher than those for $C_r = 0.8$. This level of sensitivity indicated that values specific to a given fragment/component interaction should be determined

Figure 8. Sensitivity of debris strike patterns to the number of ricochets allowed.

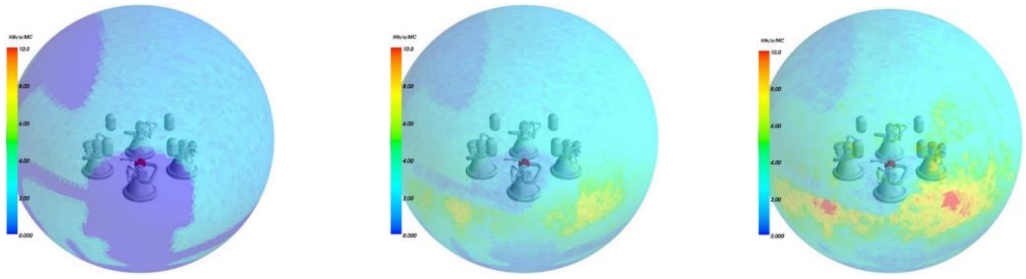

a) No propagation b) No ricochet c) With ricochet

4.3.5. Sensitivity to Blast Overpressure Failure Thresholds

One of the more difficult inputs to specify for these simulations is the level of blast overpressure that will cause component failure. For the sensitivity studies discussed in the prior sections, thresholds for peak overpressure were set to values ranging from 35 to 100 psi and those for impulse were set to 100 psi-ms (lbs/in^2 -millisecond). A deeper interrogation of the Monte Carlo results indicated that few instances were observed of blast overpressure-related component failures. A sensitivity study was conducted in which modifications to the failure thresholds of both the peak reflected overpressure and impulse were considered. This "what-if" set of runs was intended to determine levels for the overpressure thresholds at which significant blast overpressure contributions to the failure propagation would be observed.

For this study, an additional element was introduced to the configuration: a spherical tank representing one of the main propellant tanks of the stage. The size and location of the augmented configuration are depicted in Figure 9. Failure of this component resulted in the large-scale release of propellant and was considered to represent a qualitative increase in the level of risk to a crew on this vehicle. Assessing the risk according to a single component such as this allowed for a more manageable set of results, given the three-dimensional nature of the sensitivity parameter space.

Figure 9. Illustration of engine section, with fuel tank.

a. Rear view. b. Side view.

Figure 10 shows the results of this sensitivity study. The overpressure vulnerability parameters investigated are as follows:

- Peak overpressure (OP) levels of 10, 15, 35, and 100 psi with no impulse threshold (0 psi-ms). This are plotted as solid lines in Figure 10.
- Impulse levels of 20, 50, and 100 psi-ms with peak overpressure threshold of 15 psi. These are plotted as dashed lines in Figure 10.

These vulnerability combinations were applied to all energetic components, including the propellant tank component. Fragment environments and vulnerabilities were kept fixed. Each of these peak OP and impulse combinations were run for altitudes ranging from 1 km and 30 km. Since the blast overpressure scales with ambient pressure, fewer blast failures were expected at higher altitudes.

Results of each simulation were evaluated in terms of the probability of failure of the fuel tank due to blast overpressure. The overpressure failure was considered a more likely failure initiator for the low-pressure propellant tank than a fragment penetration.

Figure 10 shows propellant tank failure probability as a function of altitude for each of the vulnerability characterization combinations described. In these simulations, the blast energy scaling, (E_f), was set to 0.75; i.e., 75% of the internal energy of the failed component contribute to blast initiation. The solid lines plot the sensitivity to the peak overpressure vulnerability threshold when the impulse threshold is set to zero; i.e., failure is independent of pulse duration. Blue lines of different line style show the sensitivity to impulse. Both aspects of the blast signature were observed to be important in this case.

Figure 10. Propellant tank failure: sensitivity to altitude for various levels of blast vulnerability.

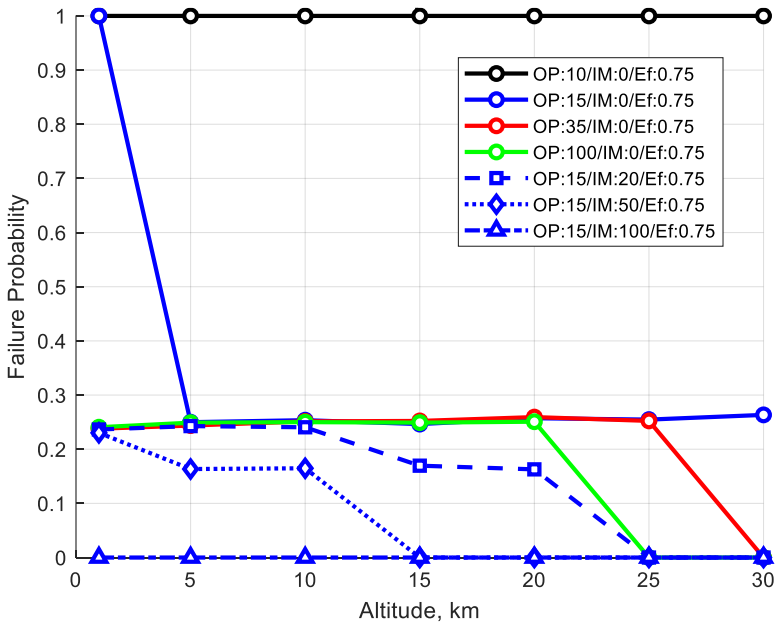

The values plotted in Figure 10 are failure probability of the fuel tank caused by blast overpressure only. Failures of other components in the propagation evolution may be due to fragment environments. In nearly all cases, the overpressure wave causing failure of the propellant tank was generated by the failure of one or more COPVs caused by either blast overpressure or fragment environments. The behavior observed in this graph can be explained in the following manner:

1) The COPVs experienced peak blast overpressures between 15 and 35 psi, even at an altitude of 30 km. This explained the sharp difference between the solid blue and red lines.
2) The COPV failures due to overpressure were effectively zero when the peak overpressure threshold was set to 35 psi and above. Therefore, the non-zero failure probabilities arise from failures of the COPV(s) due to fragment impact.
3) The additional sensitivities to altitude and vulnerability thresholds appear to be associated with overpressure-related failure of components preceding the COPV failure(s).
4) The impulse threshold was observed to impact results through its effect on the failure ratesof the COPV and of the preceding components in the failure event tree. Higher values of the

impulse failure threshold filtered out overpressure environments with high peak values and short duration.

5) Finally, the slight upward trend in the red line up to 25 km (and other lines up to the drop-off) likely resulted from the decrease in fragment drag on fragments impacting the COPVs.

For reference, the baseline impulse threshold parameter used in the previous sensitivities was 100 psi-ms (same as the dot-dash blue line). The baseline peak overpressure thresholds varied according to the component design pressure, but all were greater than 35 psi. This was the reason that the propagation in those sensitivities was dominated by fragment environments. This also highlighted the importance of the impulse threshold failure criterion, especially applications involving relatively small energy blasts imposed on nearby components.

5. CONCLUSION

Enhancements to the fragment and blast propagation models were implemented within the failure propagation simulation code described in Mathias and Motiwala [1]. The debris propagation model accounted for the effects of fragment ricochet when the impacting fragment did not cause failure of the impacted component. The integrated overpressure impulse was included as an additional failure parameter. Both peak overpressure and integrated impulse at the target component must exceed specified limits to trigger failure of the component.

Several sets of Monte Carlo simulations were computed to examine the effects of the model modifications. These results indicated the modifications had significant impact on estimated risk, represented by energetic component failure probabilities. The level of impact depended on the failure altitude and other input parameter values. Including fragment ricochet increased component failure probabilities by 30% to 50%, depending on the component. Limiting the number of ricochets allowed per fragment appeared to have minimal effect for values greater than 2 ricochets. Application of an integrated overpressure impulse substantially reduced the component failure probabilities, with the level of decrease strongly dependent on altitude. At the baseline level of impulse threshold (100 psi-ms), the failure propagation was dominated by fragment environments. However, setting the impulse threshold to zero, as in the previous version of the model, produced high likelihoods of catastrophic outcome caused by overpressure. This indicated that for this engine section, the blasts generated had high peak overpressure and very short duration.

The observed sensitivity of catastrophic outcome to the specified overpressure limits indicated a need for additional work to identify appropriate values for these inputs. There is ongoing work in support of NASA's Space Launch System using advanced hydrocodes to develop better understanding of this parameter. Other model enhancements under consideration or under active development include fragment penetration capability, functional dependence effects, and volume pressurization effects.

REFERENCES

[1] Mathias, D., & Motiwala, S. (2015). *Simulation of Liquid Rocket Engine Failure Propagation Using Self-Evolving Scenarios*. 2015 Annual Reliability and Maintainability Symposium (RAMS 2015) . Palm Harbor, FL: Institute of Electrical and Electronics Engineers (IEEE).

[2] Lundin, S., *Engine Debris Fuselage Penetration Testing, Phase 1*, DOT/FAA/AR-03/37, Dec. 2005.

[3] Lundin, S., and Mueller, R., *Advanced Aircraft Materials Engine Penetration Testing*, DOT/FAA/AR-01/27, Aug. 2001.

[4] Kingery, C. N., and Bulmash, G., *Airblast Parameters from TNT Spherical Air Burst and Hemispherical Surface Burst*, Technical Report ARBRL-TR-02555, AD-B082 713, 1984, Aberdeen Proving Ground, MD, U.S. Army Ballistic Research Laboratory.